Programming material compliance and actuation: hybrid additive fabrication of biocomposite structures for large-scale self-shaping

Bioinspiration & Biomimetics

OPEN ACCESS

PAPER

Programming material compliance and actuation: hybrid additive fabrication of biocomposite structures for large-scale self-shaping

Tiffany Cheng[1,2,*], Dylan Wood[1,2], Laura Kiesewetter[1], Eda Özdemir[1], Karen Antorveza[1] and Achim Menges[1,2]

[1] Institute for Computational Design and Construction, University of Stuttgart, Keplerstraße 11, 70174 Stuttgart, Germany
[2] Cluster of Excellence IntCDC, University of Stuttgart, Keplerstraße 11, 70174 Stuttgart, Germany
[*] Author to whom any correspondence should be addressed.

E-mail: tiffany.cheng@icd.uni-stuttgart.de

RECEIVED
15 April 2021

REVISED
8 June 2021

ACCEPTED FOR PUBLICATION
1 July 2021

PUBLISHED
26 July 2021

Keywords: computational design, 3D printing, mechanical metamaterials, bio-based materials, bio-inspired engineering, autonomous systems, adaptive architecture

Supplementary material for this article is available online

Abstract

We present a hybrid approach to manufacturing a new class of large-scale self-shaping structures through a method of additive fabrication combining fused granular fabrication (FGF) and integrated hygroscopic wood actuators (HWAs). Wood materials naturally change shape with high forces in response to moisture stimuli. The strength and simplicity of this actuation make the material suitable for self-shaping architectural-scale components. However, the anisotropic composition of wood, which enables this inherent behavior, cannot be fully customized within existing stock. On the other hand, FGF allows for the design of large physical parts with multi-functional interior substructures as inspired by many biological materials. We propose to encode passively actuated movement into physical structures by integrating HWAs within 3D-printed meta-structures with functionally graded stiffnesses. By leveraging robotic manufacturing platforms, self-shaping biocomposite material systems can be upscaled with variable resolutions and at high volumes, resulting in large-scale structures capable of transforming from flat to curved simply through changes in relative humidity.

1. Introduction

Wood is a sustainable, readily available, easily machinable, and high-performance construction material with a long history of human usage. Naturally, wood is also hygroscopic; fluctuations in moisture result in swelling and shrinking. This capacity to change shape is inherent to the material's biological structure, and continues to occur even as dead tissue long after harvesting (Eder *et al* 2020). Ancient Egyptians have exploited wood's dimensional instability to split rocks through the wetting of wooden wedges, achieving high enough swelling forces to fracture granite weighing over two metric tons while requiring no motors or electrical energy (El-Sehily 2016). Nonetheless, the hygroscopicity of wood often results in unwanted deformation during manufacturing and throughout the course of the material's use, and is thus commonly perceived as a major deficiency. In fact, tremendous effort and energy are dedicated to suppressing this moisture-induced behavior in industry through kiln drying and extensive modification processes (Breiner *et al* 1987 and Bergman and Bowe 2008).

In nature, however, a wide range of materials employ hygroscopicity to advantageously change shape, simply in response to environmental stimuli. One example is the Pinaceae conifer cone: without consuming any metabolic energy, its scales have been observed to open when suitably dry for seed dispersal, while remaining closed when damp. Due to their complex anisotropic structuring of hygroscopic cells and tissues, cones of the pine family (e.g. pines and spruces) react to changes in climatic conditions with autonomous movements (Harlow *et al* 1964 and Dawson *et al* 1997). Even after detaching from the tree

millions of years ago, ancient but well-preserved cones can still continue to open and close (Poppinga *et al* 2017).

By drawing inspiration from nature and embracing wood's hygroscopic and orthotropic behavior, wood can be harnessed to become a natural actuator. In a cross-ply bilayer configuration, moisture-induced changes in shape are converted into curvature through bending (Rüggeberg and Burgert 2015). This adaptiveness alludes to the potential for self-forming building components or weather-responsive facade elements (Vailati *et al* 2018). Bilayers crafted from maple wood veneer and epoxy-bonded glass fiber composite have been studied to reversibly and reliably bend in response to relative humidity (RH) fluctuations (Reichert *et al* 2015). At increased size and thickness, bilayers constructed from beech and spruce wood have been proven for the manufacturing of curved mass timber components (Grönquist *et al* 2019) and self-erecting of multi-part mechanisms such as gridshell structures (Grönquist *et al* 2020).

These bio-inspired wood bilayers showcase how a biological material can be designed and engineered as an integrated sensor, actuator, and controller (Menges and Reichert 2015). However, when compared to the pine cone, they still lack the functional gradation and complex movements occurring from a highly differentiated structure. The structural properties of wood specific to shrinking and swelling can be adjusted globally through densification, delignification, or chemical treatment (Frey *et al* 2018 and Grönquist *et al* 2019). As a natural material, however, its intrinsically stark anisotropy cannot be fully customized within raw logs or sawn stock. Tailoring the direction of hygroscopic actuation can be achieved by additively combining multiple boards into larger parts as a discrete approximation (Wood *et al* 2016 and Wood *et al* 2018). Still, due to the existing structure of the material, there are limits to the resolution of variations in actuation as well as stiffness; moreover, these properties cannot be entirely decoupled when using wood as the sole material.

In parallel, additive manufacturing has emerged as a popular digital fabrication technique for creating geometrically complex shapes with precision and repeatability. Additive processes have been demonstrated at larger scales through timber as a structural material for building non-standardized architectural components (Willmann *et al* 2016 and Thoma *et al* 2019). At smaller scales, this technology has enabled the manufacturing of compliant mechanisms with tunable deformation behaviors (Megaro *et al* 2017) and mechanical meta-materials with a range of elasticities (Panetta *et al* 2015). Interestingly, extrusion-based 3D-printing produces anisotropy through the paths of material deposition, which can be numerically controlled to affect the mechanical properties (Raney and Lewis 2015). Using stimuli-responsive materials, matter can even be programmed to change shape (Tibbits 2014, Correa *et al* 2015, Tahouni *et al* 2020 and Langhansl *et al* 2021), but these laboratory-scale prototypes generally lack the high swelling force and actuation speed necessary for some applications (e.g. upscaling for buildings). Compared to other moisture-reactive and bio-based materials, wood retains its stiffness remarkably well (Rowell 2012).

2. Research aim

Whereas wood is responsive and multiple boards can be combined to build large structures quickly, 3D-printing is slow for building volume but can produce a high resolution of detail. Thus, an integrative multi-material approach utilizing dual processes can achieve the scale and actuation strength of wood bilayers while maintaining the physical programmability that extrusion-based 3D-printing enables. In this paper, we present a hybrid fabrication method for producing large-scale self-shaping biocomposite material systems by combining shape-changing *hygroscopic wood actuators* (HWAs) with *3D-printed meta-structures* of customized properties and complimentary functionalities (figure 1).

We first introduce our integrated computational design and hybrid additive fabrication strategy. The production set-up features an industrial six-axis robotic arm for the fused granular fabrication (FGF) of 3D-printed meta-structures, as well as the tooling and placement of pre-manufactured HWAs. We program the actuation and compliance of large self-shaping structures through the strategic placement of the HWAs and by modulating the geometry and quality of extrusion. We evaluate the effect of mesoscale functional patterns on macroscale objects and assess the tectonic integration between the natural and meta-materials, both bio-based. Finally, we produce 300 cm long components with thicknesses up to 8 cm, which are capable of tailored self-shaping at a large scale.

3. Methods in material programming

3.1. Integrative computational design

Combining multiple materials and processes to create a self-shaping biocomposite material system at large-scale calls for integrative strategies in what we term material programming.

We developed a parametric model for defining areas of *active actuation* and areas with *passive properties* (Cheng *et al* 2020). Individual HWAs are represented by discrete areas of active actuation, each delineated by its overall dimensions when flat as well as its orientation, direction, and amount of bending. The 3D-printed meta-structure is represented by a continuous area of passive properties, whose variable

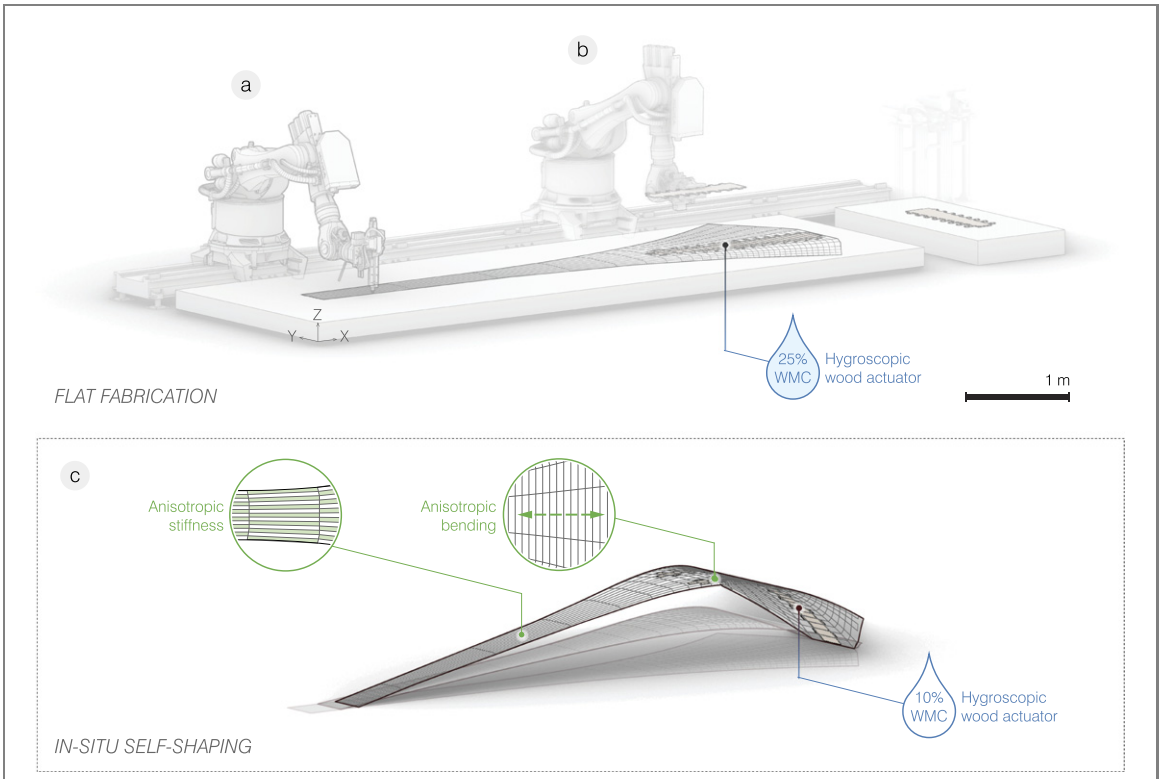

Figure 1. Biocomposite structures are fabricated in the flat state via a hybrid additive fabrication sequence. (a) Using an industrial robotic arm, compliance is tailored at varying magnitudes and anisotropies through FGF; (b) after a tool change, actuation is programmed by inserting HWAs with 25% WMC. (c) The components are then deployed in ambient conditions, resulting in self-shaping at the meter scale as the HWAs equalize to a WMC of 10%.

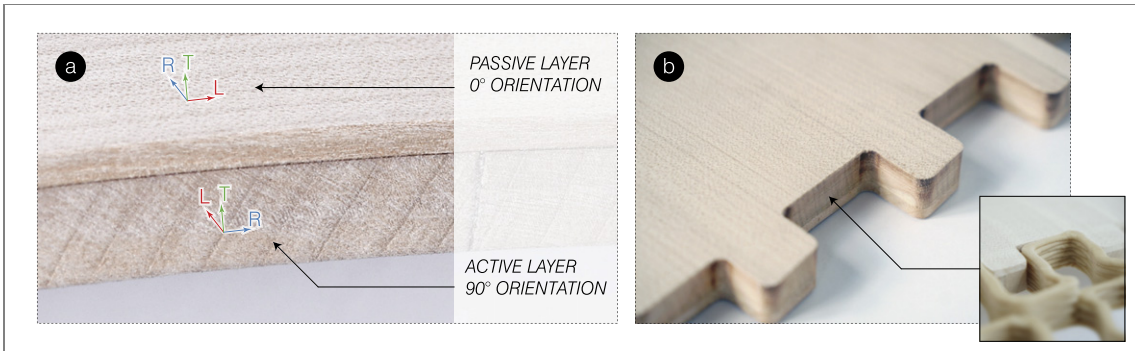

Figure 2. (a) The HWA is comprised of a passive layer oriented 0° and an active layer oriented 90°, resulting in the respective radial (R), tangential (T), and longitudinal (L) directions (±15° depending on the sawn stock) of each bilayer element. (b) HWAs are detailed for each biocomposite design with toothed-edges surrounding their extremities, which fill the neighboring cells of the 3D-printed meta-structure.

compliance and anisotropy depend on its distribution of mesoscale functional patterns. In manufacturing, mesoscale is defined as being situated between microscopic and macroscopic length scales (Dow and Scattergood 2003); here, we are referring to the internal topology and underlying structure of a bulk component. Based on the meta-structure design and 3D-printing constraints described in section 3.2, FGF inherently encodes artificial properties into the material system, extensive of their material composition (Redlich 1970). In section 3.4, we describe the test set-up for studying these properties and determining the programming parameters for controlling compliance and actuation.

Biocomposite designs are modeled using a visual programming environment (`Grasshopper 3D`, Build 1.0.0007) running within a computer-aided design software (`Rhinoceros 3D`, version 6 SR13). The meta-structure is generated by analyzing local, spatial changes in geometry between the flat surface and the shaped surface and then mapping functional patterns according to their target distortions. This meta-structure design is then converted to 3D-printable machine instructions, which dictate the trajectory and quality of extrusion. The physical HWAs were pre-manufactured for the hybrid additive fabrication process, their preparation explained in section 3.2. Thus, voids are left in the

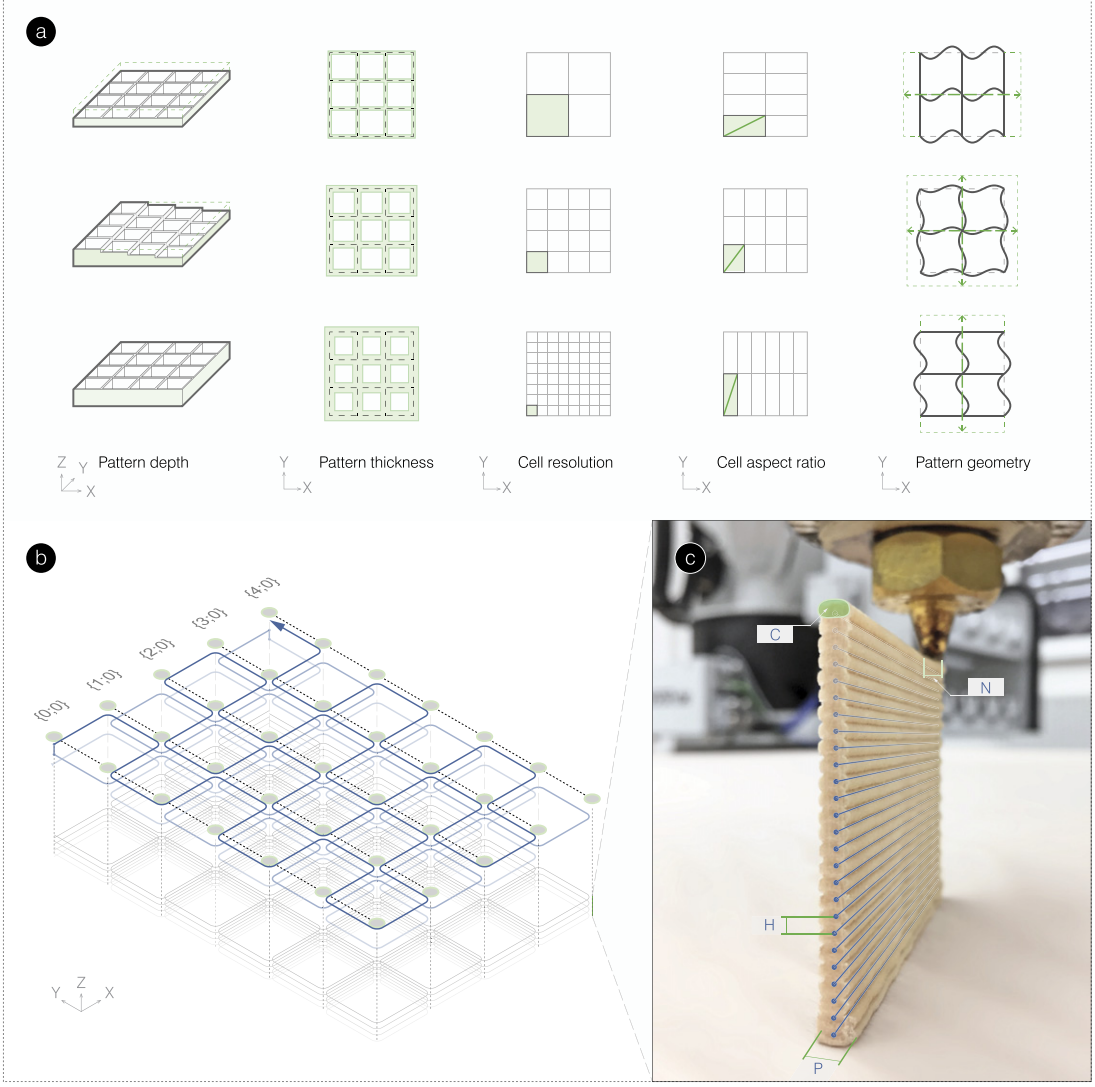

Figure 3. (a) Mesoscale functional patterns are customizable through modulating the depth, thickness, resolution, aspect ratio, and geometry parameters. (b) Multi-layered, crossing, zig-zag toolpaths can be applied to any structured grid. (c) The nozzle diameter constraint *N* and layer height parameter *H* are the primary factors in the resulting bead cross-section *C* and path width *P* extrusion properties.

meta-structure to indicate their locations for the later insertion phase. Prior to the robotic fabrication process (described in section 3.3), we simulated the robotic toolpaths digitally as well as physically tested the extrusion and insertion sequence on a desktop fused filament fabrication 3D-printer (FELIX Tec 4 Dual Head, FELIXprinters, Utrecht, Netherlands).

3.2. Natural and meta-materials

3.2.1. Hygroscopic wood actuator

For each biocomposite test and prototype, we pre-manufactured the HWAs in standardized, rectilinear, cross-ply, double-layered plates. Each plate was constructed from a thicker active layer of boards and a thinner passive layer of boards, arranged perpendicular to one another (table A1). The bilayer configuration was based on an estimated range of desired curvatures and structural capacity (details in appendix A).

Boards for the active layer were sourced from a local carpentry mill, pre-cut into individual elements for assembly, and then placed in adsorption at 95% RH to raise their WMC; in the case that boards could be sourced directly from a sawmill close to the time of harvesting, they were placed in desorption at 95% RH to lower the WMC from the green state. Equalization was achieved by storing the boards in a humidity-controlled (MiniOne Humidity Generator, Preservatech, Bydgoszcz, Poland) custom-built chamber, while monitoring their WMC with a fixed resistance sensor data logger (Hygrofox, Scanntronik, Zorneding, Germany). After reaching a WMC of 25%, the boards were planned down to the desired thickness and edge-glued to create an active layer.

Boards for the passive layer were sourced, already cut and planned to final dimensions for assembly, and stored to maintain a low WMC. The high WMC active layer and low WMC passive layer were then laminated

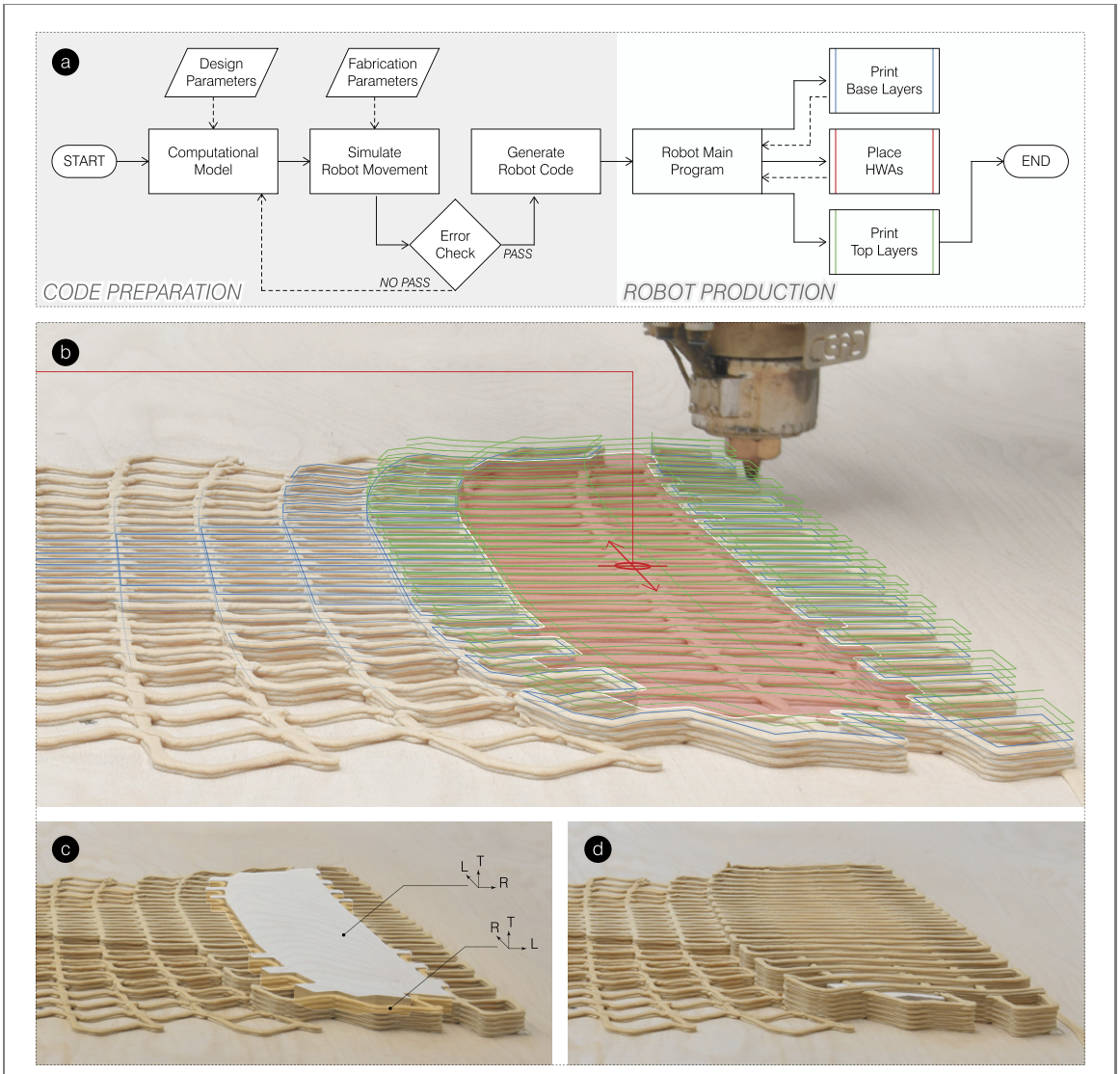

Figure 4. (a) A process chart of the computational design workflow for hybrid additive fabrication; design and fabrication parameters are input to generate the main robot program and subroutines (details in appendix B). (b) The coordinated production sequence of one biocomposite component; the blue, red, and green toolpaths respectively represent the 3D-printing of the meta-structure's base layers (shown here in the midst of production), placing of the HWA, and 3D-printing of the meta-structure's top layers. (c) The same biocomposite component after HWA insertion, (d) and with the HWA fully embedded.

together with a one-component polyurethane adhesive (LOCTITE HB S309 PURBOND, Henkel, Sempach Station, Switzerland) and pressed in a vacuum bag. After curing, each specific HWA was cut from the bilayer sheets using a three-axis computer numerical control milling machine (figure 2). The finished HWAs were kept in a sealed container and covered with moist towels to maintain a flat geometry until the robotic placement procedure.

3.2.2. 3D-printed meta-structure

Mesoscale features are inevitably imprinted onto the 3D-printed meta-structure and affected by the layer-by-layer extrusion process. These features can be customized by controlling the geometric trajectory of the toolpath, as well as by fine-tuning the speed of printing and flow of material (Cheng *et al* 2020).

The 3D-printed meta-structure is structured as a grid that can vary in density and angle between the X- and Y-axes, as well as in the pattern geometry of each cell (figure 3(a)). By modulating the pattern geometry, as well as the resolution and aspect ratio of the basic cell unit in the XY-plane, passive properties such as compliance and bending stiffness can be customized at varying magnitudes and anisotropies; furthermore, the thickness of the pattern can be tuned by controlling the width of extruded paths via the flow of material during extrusion. The pattern depth is adjusted through the number of printed layers in the Z-axis. As a continuous path of material deposition provides the best possible mechanical performance, we formulated a path-planning logic for multi-layered crossing zig-zag toolpaths (figure 3(b)).

The finest resolution of detail that can be achieved is constrained by the nozzle size of the extruder (figure 3(c)). We used a 3 mm diameter nozzle and printed all layers with a height of 2 mm, producing extruded paths with a bead width of

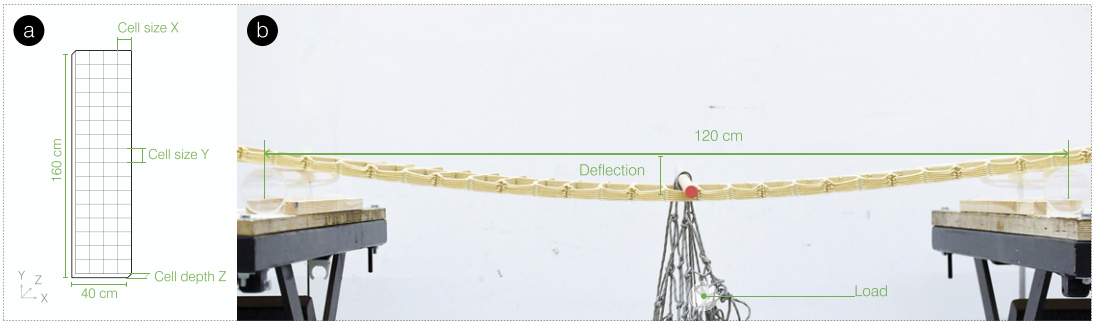

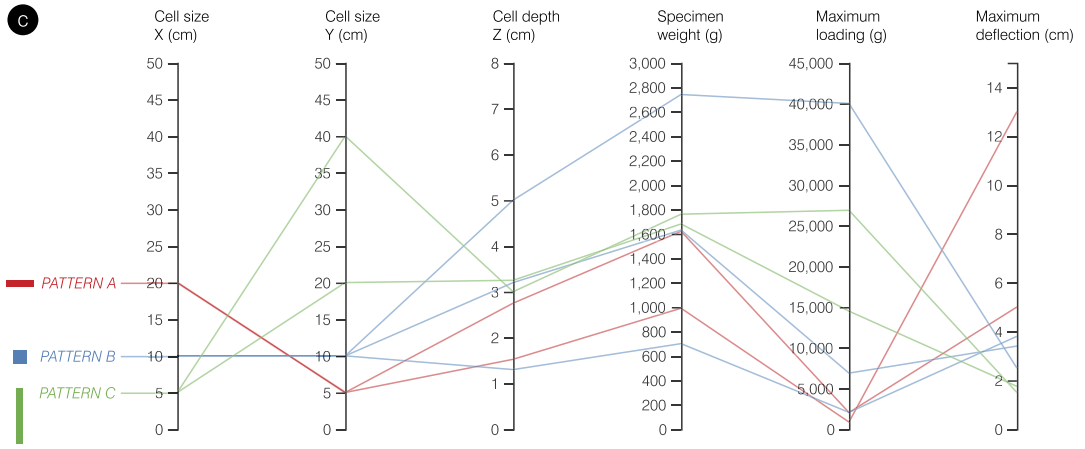

Coupon type	Cell size X (cm)	Cell size Y (cm)	Cell depth Z (cm)	Specimen weight (g)	Maximum loading (g)	Maximum deflection (cm)
PATTERN A	*20*	*5*	*1.525*	*990*	*870*	*13.0 ± 1.75*
PATTERN A	*20*	*5*	*2.75*	*1,620*	*2,040*	*5.0 ± 0.8*
PATTERN B	*10*	*10*	*1.3*	*700*	*2,060*	*3.8 ± 0.4*
PATTERN B	*10*	*10*	*3.2*	*1,630*	*6,880*	*3.4 ± 0.3*
PATTERN B	*10*	*10*	*5*	*2,740*	*40,000*	*2.5 ± 0.4*
PATTERN C	*5*	*20*	*3.25*	*1,680*	*14,490*	*1.8 ± 0.05*
PATTERN C	*5*	*40*	*3*	*1,760*	*26,880*	*1.5 ± 0.09*

Figure 5. (a) Functional patterns were studied in coupons with variations in the three Cartesian coordinates. (b) The set-up of the three-point flexural test spans 120 cm; each coupon was loaded incrementally and its deflections were measured. (c) Visualized here are correlations among pattern types with X-axis anisotropy (red), isotropy (blue), and Y-axis anisotropy (green). The data shows a negative, inverted relationship between the maximum allowable deflection and the maximum loading before failure.

6 ± 0.25 mm and cross-section of 11.14 mm^2 when printed at 125 mm s^{-1} (the first layer was printed 1 mm above the build plate and at 75 mm s^{-1} to maximize adhesion and surface area contact). The material flow was automatically mapped in relation to the printing speed for maintaining the target bead cross-section, with small adjustments to the bead cross-section made through a multiplier.

We produced the meta-structure through the extrusion of granular pellets developed specifically for FGF. The granular pellets were made from a cellulose-filled bio-based polylactic acid compound (UPM Formi 3D 20/19, UPM Biocomposites, Lahti, Finland). The material was chosen for its cellulose fibers (20% fiber content), which help to prevent the creation of internal stresses; moreover, the material can be post-processed similarly to wood.

Prior to fabrication, the granular pellets were stored in cool and dry conditions. Just before printing, the pellets were dried at 80 °C for at least 3 h in a dehumidifying dryer (DRYPLUS, VISMEC, Camposampiero, Italy). During printing, the material was transported directly from the dryer through four heat zones, starting from a first temperature of 160 °C and finally extruded through the nozzle at a temperature of 190 °C.

3.3. Robotic platform for hybrid additive fabrication

The biocomposite components were fabricated in a production hall utilizing a six-axis industrial robotic arm (KUKA Fortec KR420 R3080) on a 12 m linear track. The robotic arm was equipped with multiple interchangeable end-effectors: a robotic extrusion

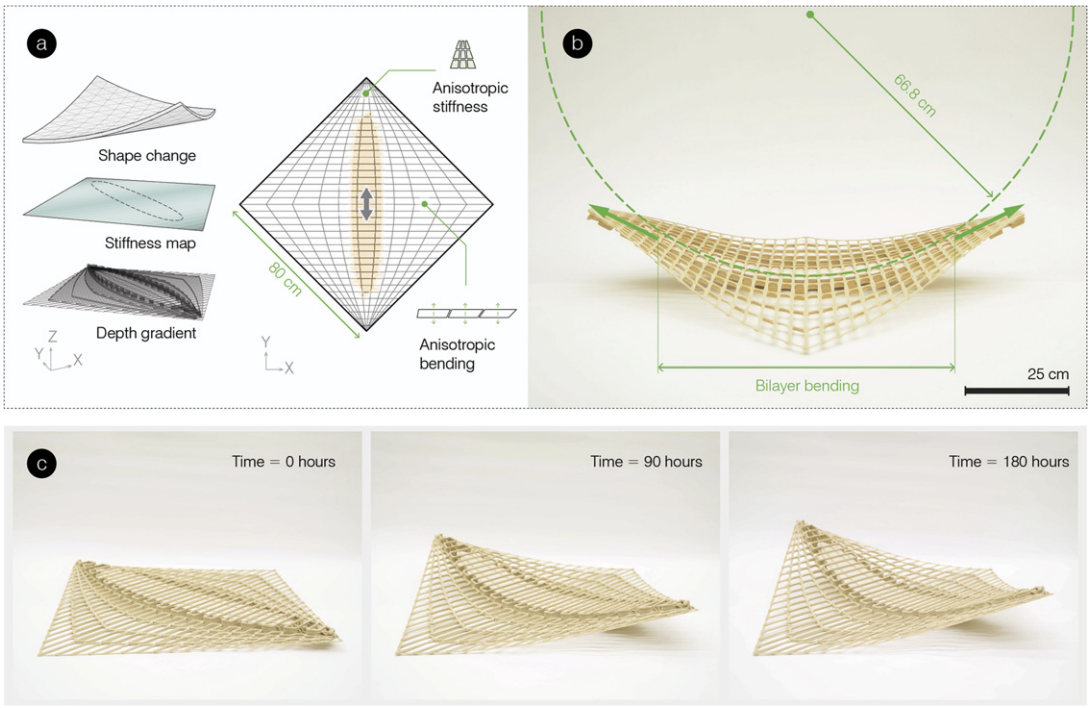

Figure 6. (a) The material programming of a biocomposite specimen with a single HWA; it was designed to bend in one direction. (b) A specimen with its HWA inserted in the convex direction during fabrication; it was allowed to self-shape in the concave direction (see supplementary video 1 https://stacks.iop.org/BB/16/055004/mmedia), which resulted in a 66.8 cm bending radius. (c) Shown here are time-lapse stills from the self-shaping of a specimen with its HWA inserted in the concave direction during fabrication, resulting in a 57.9 cm bending radius.

system for the FGF of thermoplastic granular pellets (Robot Extruder, CEAD, Delft, Netherlands) and a vacuum gripper for handling planar HWAs (vacuum area gripping system, Schmalz, Glatten, Germany). The production set-up included a quick tool change adapter system (Change System, SCHUNK, Lauffen am Neckar, Germany), allowing the two methods of additive fabrication to be fully integrated together (figure 4(b)).

We produced the biocomposite components in one robotic fabrication procedure that incorporated several automation subroutines. On a non-heated build plate table with a workspace of 300 cm × 150 cm (extendable to 1200 cm × 200 cm), the base of the meta-structure was first 3D-printed with voids for indicating the positions of the HWAs. During especially lengthy fabrication sessions, the meta-structure was outfitted with 3D-printed tabs for mechanical fastening in order to prevent delamination from the build plate. After reaching the depth of the HWAs, a tool change was called to initiate the pick-and-place sequence. The planar HWAs were individually retrieved from a feeding tray to the workspace, then rotated to the correct orientation and inserted. After insertion into the meta-structure, a tool change was called for reverting back to the 3D-printing sequence. As the humidity and temperature were not easily regulated in the production hall, a limited time window remained for encasing the HWA, which risked actuating during the final phase of fabrication unless mechanically fastened.

The process of preparing and generating the robot code is shown in figure 4(a), and the technical details of the code organization are described in appendix B.

3.4. Testing and evaluation

To gain an understanding of the programmable material properties, we performed several experiments. In one parameter study, several coupons of the 3D-printed meta-structures were subject to a three-point flexural test spanning a length of 120 cm (figure 5(b)), with their deflections logged at each loading step until failure. The measurements were plotted on a parallel coordinates graph for visualizing the relationships between various combinations of the material programming parameters and their flexibility or ability to resist bending. For each pattern, we produced three coupons with the dimensions 160 cm × 40 cm and averaged the results. Both fabrication and testing occurred in the production hall with environmental conditions of 23 °C and 38%–39% RH.

In another study, we evaluated the tectonic integration between the natural and meta-materials. We produced a series of specimens with varying arrangements of HWAs embedded within the 3D-printed meta-structure. Immediately after fabrication, each specimen was transported to the actuation environment along with a naked, unembedded HWA as the control. The self-shaping process was captured by time-lapse photography (Nikon D7100 DSLR camera with Camera Control Pro 2 software) at an interval of 15 min. At approximately the seventh day of

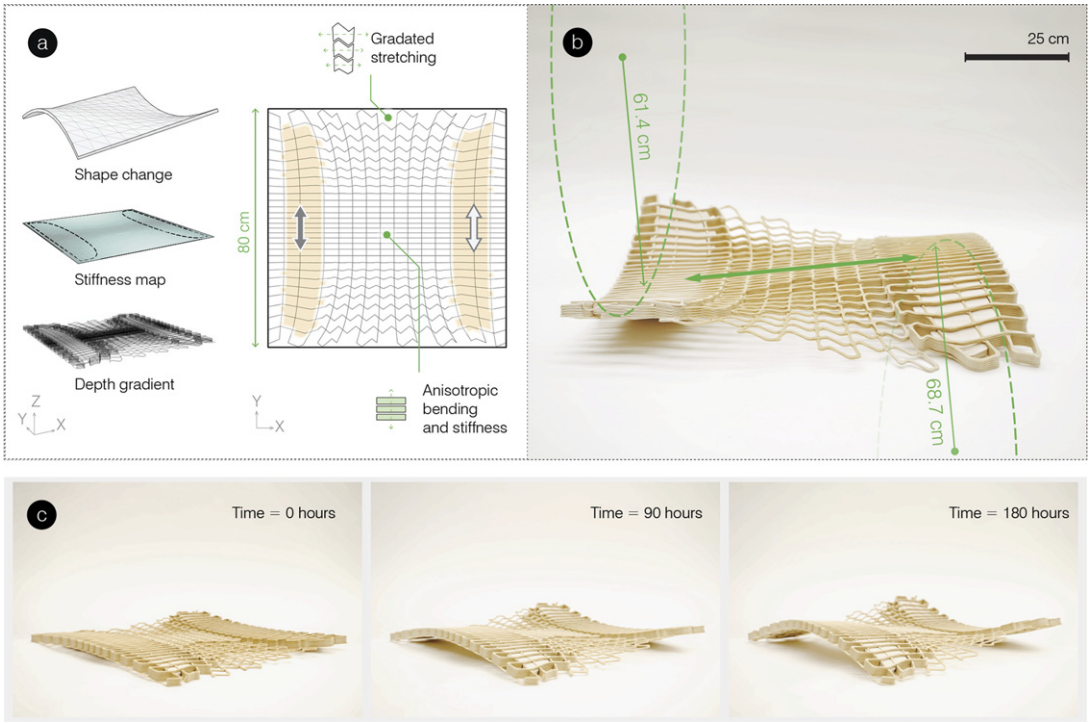

Figure 7. (a) The material programming of a biocomposite specimen with a pair of HWAs aligned parallel to each other; it was designed with high stiffness along the center beam that bridges the HWAs, and low stiffness at the edges for allowing the HWAs to bend in alternating directions. (b) The concave HWA on the left side achieved a 61.4 cm bending radius, while the convex HWA on the right side achieved 68.7 cm (see supplementary video 2). (c) Shown here are time-lapse stills from the self-shaping of a specimen with its HWAs inserted in the opposite directions.

equalizing to indoor conditions regulated to 30% RH at 21 °C to 23 °C (WMC measured by fixed resistance moisture meter), the bending radii were calculated from the measured chord length and sagitta and then compared to the naked HWA. For each design, we produced three specimens with the size of 80 cm × 80 cm and averaged the results.

4. Self-shaping biocomposite material system

4.1. Programmed compliance via mesoscale functional patterns

We measured the effects of the mesoscale functional patterns on bending behavior. Three categories of functional patterns were produced: patterns with anisotropy in the X-axis, isotropic patterns, and patterns with anisotropy in the Y-axis (figure 5(a)). In general, we were able to tune the compliance across a wide range (figure 5(c)). A high amount of flexibility could be attained (with the maximum deflection measured at 13 cm); yet, using the same material but in a different pattern, the bending stiffness could be increased to resist loads up to 40 kg.

In one series of sample tests, the patterns were kept constant but with varying depths. This was achieved simply by adjusting the number of printed layers along the Z-axis. The results in this series showed that raising the depth was very effective at increasing bending stiffness, while also drastically increasing the weight. Bending stiffness could also be increased without changing the overall depth via higher resolutions of the pattern, but increases the density and therefore the weight.

In another series of sample tests, the weight and depth of all coupons were kept constant (within 5%) with variations in the pattern occurring on the XY-plane. This was achieved by calculating the total length of the printed path, and adjusting the number of cells in the X- and Y-axes to maintain the same length and number of layers (and thus weight and depth, respectively). These results showed a positive correlation between anisotropy in the Y-axis, the direction of spanning, with the maximum allowable load before failure. Therefore, strength could be achieved in a specific direction without adding significant weight.

4.2. Tectonic integration with embedded hygroscopic wood actuators

The biocomposite components gain their self-shaping abilities through the HWAs embedded within the 3D-printed meta-structures. Although performing distinct functions, each material is programmed to behave in relation to the other and function together as a holistic entity. Essentially acting as an exoskeleton, the meta-structure should be flexible enough to permit bending in the same direction as the HWA, while at the same time strong enough to contain the HWA and extend its area of influence (e.g. by

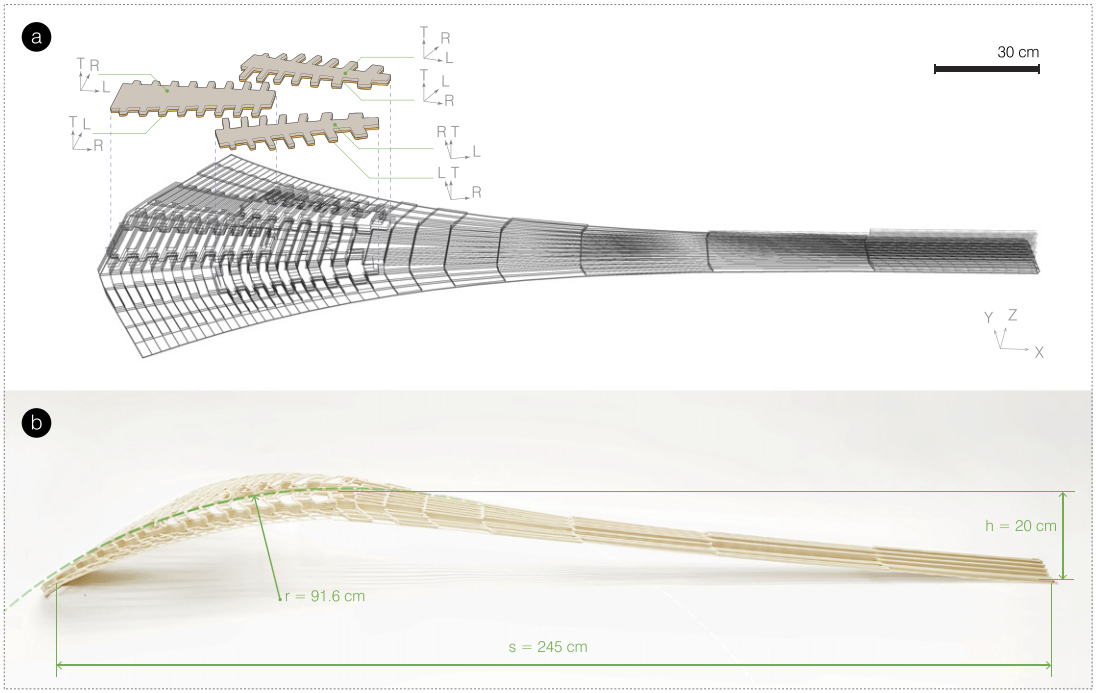

Figure 8. (a) The design for an asymmetrical arch was fabricated with an overall footprint of 300 cm × 90 cm. Curvature on one side was programmed via the insertion of HWAs, shown here with the radial (R), tangential (T), and longitudinal (L) directions of the bilayer elements indicated. High bending stiffness at the other end was programmed via the 3D-printed meta-structure. (b) After equalizing to ambient conditions, the biocomposite prototype reached a height of 20 cm, demonstrating self-shaping at large-scale.

transferring loads in the direction orthogonal to bending).

We designed the HWAs with toothed-edges surrounding the extremities, which fill the neighboring cells of the 3D-printed meta-structure (figure 2(b)). Besides increasing the surface area for an interference fit, these teeth create additional points for the encapsulating 3D-printed layers to grip, resulting in a stronger bond between the two materials. We found that increasing the material flow of the 3D-printed meta-structure surrounding the HWAs aided in preventing damage due to stress concentrations where the two materials interface. Without the teeth attachment geometry or fortified 3D-printing for securely embedding the HWAs, the HWAs were observed to break through the 3D-printed meta-structure in some specimens; therefore all of the tested specimens in the following study incorporated these features.

We produced two types of biocomposite specimens: a design with a single HWA (figure 6(a)) and a design with a pair of HWAs aligned parallel to each other in alternating directions (figure 7(a)). To assess the interaction between the two materials, we measured the bending radius of each HWA in the different samples. In general, we were able to cause the entire surface to change shape (see supplementary videos 1-2 (https://stacks.iop.org/BB/16/055004/mmedia)); the objective was to achieve unhindered bending with a radius as close as possible to the naked HWA.

The HWAs were observed to equalize to the target WMC of 10% after about 160 h. Without the 3D-printed meta-structure, the naked HWAs had an average bending radius of 49.5 cm when self-shaping in the concave direction (with the active layer on top). It was observed that the naked HWAs had an average bending radius of 52.4 cm when self-shaping in the convex direction (with the active layer on bottom), presumably from additional resistance in the form of self-weight.

In both designs, there was a gradient in the pattern depth for tuning stiffness; because of the layer-by-layer extrusion process, the gradient occurs only on the upper layers. For the single HWA biocomposite design, we compared specimens with the HWA inserted in opposite directions. The specimen with the HWA inserted in the concave direction exhibited a bending radius of 57.9 cm (figure 6(c)), while the specimen with the HWA inserted in the convex direction exhibited a bending radius of 66.8 cm (figure 6(b)). We infer this to be because the side with depth gradient is allowed to contract or expand more easily; as the HWA's active layer shrinks in equalization to ambient RH, it should be positioned on top in the concave direction. This postulation was corroborated by the double HWA biocomposite specimens, in which two variations with opposite bending directions were compared (figures 7(b) and (c)). In both cases, the concave HWAs achieved a bending radius of 61.4 cm, tighter than that of the convex HWAs measured at 68.7 cm.

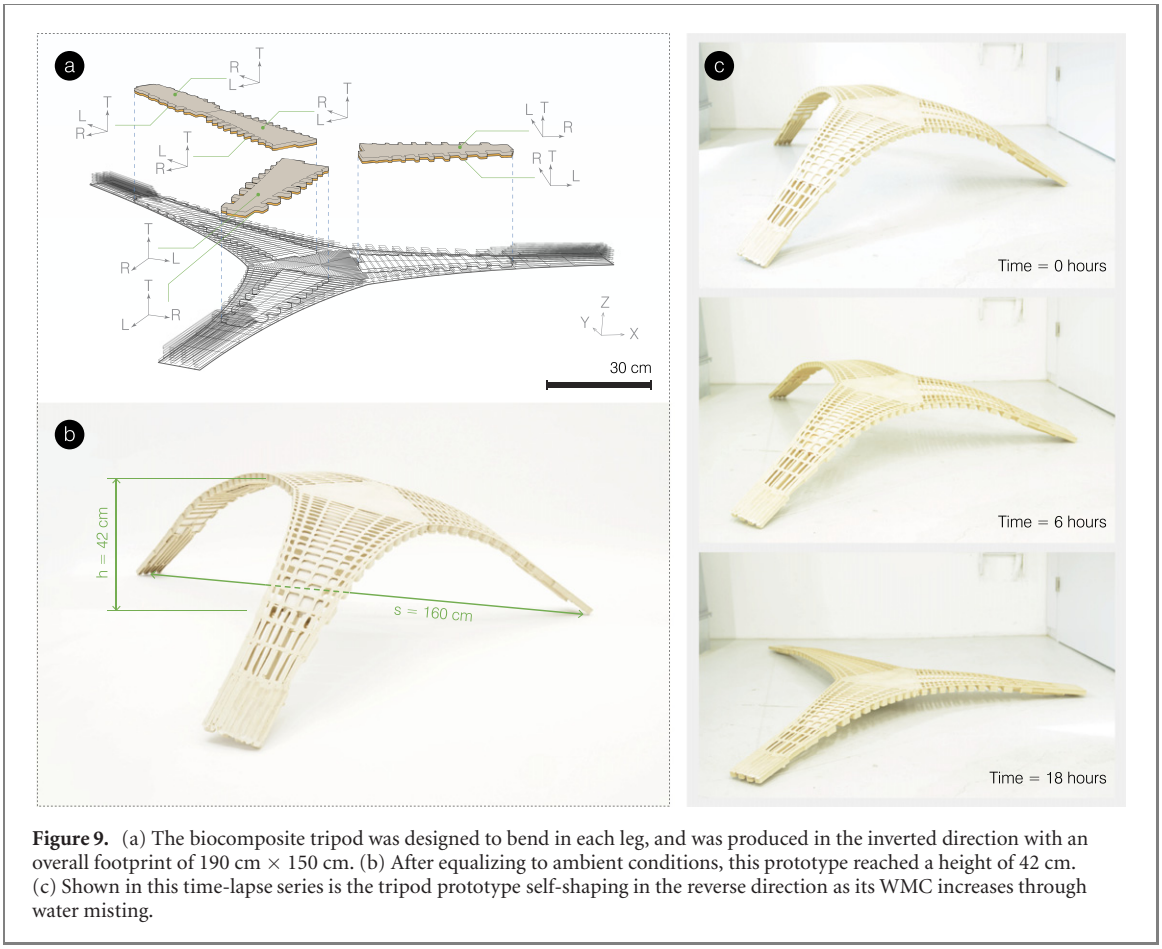

Figure 9. (a) The biocomposite tripod was designed to bend in each leg, and was produced in the inverted direction with an overall footprint of 190 cm × 150 cm. (b) After equalizing to ambient conditions, this prototype reached a height of 42 cm. (c) Shown in this time-lapse series is the tripod prototype self-shaping in the reverse direction as its WMC increases through water misting.

4.3. Full-scale deployment via robotic fabrication

As a demonstration of this approach, we deployed our hybrid additive fabrication strategy at full-scale to produce a set of larger biocomposite prototypes. We designed these prototypes by synthesizing our findings from the previous sections.

The first biocomposite prototype was a long-spanning geometry that was designed to bend at one end in creating an asymmetrical arch (figure 8) from an initial overall footprint of 300 cm × 90 cm. To create curvature, one side was programmed with three HWAs, while the meta-structure on the other side was programmed with depths up to 8 cm to promote stiffness. The fabricated prototype weighed 4.5 kg; after self-shaping for 180 h, the biocomposite arch achieved a bending radius of 91.6 cm, reaching a height of 20 cm and spanning a total distance of 245 cm.

The second biocomposite prototype was a three-legged geometry that was programmed to bend in each of the 85 cm to 140 cm long legs, creating a tripod structure (figure 9). This prototype was fabricated with an overall footprint of 190 cm × 150 cm. It was designed with two shorter legs and one longer leg with an additional HWA; the meta-structure was designed as an exoskeleton with depths up to 5 cm for joining all the areas. The resultant prototype weighed 4.8 kg; after self-shaping for 180 h, the biocomposite tripod reached a height of 42 cm, spanning a distance of 160 cm between the long and short legs.

The biocomposite structures were intended to self-erect from their initially flat states. After 72 h of equalization to ambient RH, the HWAs of both prototypes were observed to have notably less curvature than the naked HWA. As the scale had significantly increased from the previous specimens, it was evident that both 3D-printed meta-structure and HWAs had difficulty self-erecting with the added weight. Although the 3D-printed meta-structure was able to accommodate the HWAs with high flexibility in the bending areas, it lacked enough stiffness in the remaining areas to lift the entire structure while the HWAs self-shaped in the convex direction; furthermore, the mechanical linkage of the 3D-printed meta-structure to the HWAs exhibited high bond stresses from the increased forces. The prototypes were flipped over to self-shape in the concave direction, reducing the lifting load; the self-shaping process was then accelerated, and the HWAs embedded within the tripod prototype achieved an average bending radius of 77.5 cm after equalization.

5. Discussion

Our results indicate the benefits of leveraging the autonomous actuation of wood bilayers with the

tailoring of mechanical properties enabled by 3D-printing. Related work in hybrid additive manufacturing has shown that it is possible to 3D-print a working quadcopter drone with an embedded motherboard and other electronic parts (Lewis *et al* 2016 and Valentine *et al* 2017). But in place of electronics and digital control, we encode movement in the *physical material* and *fabrication logic* using stimuli-responsive actuators. While our biocomposite material system achieves adaptivity through changes in its curvature and structure, there are still a number of open questions.

The first topic for future work is the interface between the HWAs and 3D-printed meta-structure, as they are two separate materials serving distinct roles within the system. The robotic fabrication platform can be extended to include subtractive tooling along with the additive extrusion and placement processes for better fit and precision; both the HWAs and 3D-printed meta-structure can be shaped to incorporate high-resolution features for increased grip and friction. In addition, the automated application of adhesives can also improve the connection between natural and meta-materials; this inclusion could also lend itself to the future in-situ construction of the HWAs during the robotic procedure (instead of pre-manufacturing them prior to hybrid additive fabrication), opening the design space to more continuous material distributions.

For further upscaling, the resultant increase in the structure's self-weight becomes exceedingly important at larger scales. It will be critical to consider the structural mechanics of self-shaping biocomposite structures by simulating their movement and adaptive loading for multiple structural conditions. Higher actuation forces might be attained by employing thicker HWAs for increased structural depth and stiffness, as well as a redundancy of HWAs in the system to distribute the load across many actuators. Especially during the self-erecting process, it will be necessary to capitalize on 3D-printing's ability to tune the ratio between strength to weight. As the programming of the meta-structure behavior is dependent on a multitude of geometrical and physical parameters, (re)calibration to the chosen material is required when new functional patterns are used. This might be alleviated by the inclusion of finite element analysis for an improved prediction and mechanical model of the meta-structure pattern and behavior.

Although we have shown self-shaping at a large scale, the adoption of biocomposite material systems in architecture will require further investigation. In the case of irreversible self-shaping (e.g. in deployable structures and shells), safety mechanisms will need to be examined. Potential 3D-printed functions for blocking shape changes and locking the desired structure may mitigate the competing criteria between flexibility (during the shape change) and stiffness (for structure after the transformation). Auxetic mechanisms present promising opportunities for generating double curvature through changing Gaussian curvatures (La Magna and Knippers 2018). We are particularly interested in surveying the additional functionalities which are enabled by hybrid additive fabrication, such as spatial arrangement (e.g. vertically oriented or tilted HWAs), stacking and layering of HWAs in the Z-axis, and differentiated distribution of passive and active wood elements within the 3D-printed meta-structure.

For the application of weather-responsive facades that can manage the indoor climate, the biggest challenge is increasing actuation speeds by overcoming the poroelastic time scale (Poppinga *et al* 2018). Exploring geometries with increased surface area to volume ratio (e.g. discretized and distributed HWAs with decreased width but preserved length and depth) might offer better exposure and sensitivity to their environment. Still, a change in material would be required after the geometrical and spatial limits are reached. In scenarios requiring a high degree of control over timing and duration (e.g. for shape changes centered around the changing needs and schedules of building occupants), it is possible to further fine-tune biocomposite behavior by regulating its microclimate. Temperature and RH, as a function of absolute moisture and air temperature, are interrelated; as such, heat could be harnessed to manipulate local RH to desired conditions by capitalizing on the thermal mass of the building envelope.

6. Conclusion

We have demonstrated the capacity of self-shaping biocomposite material systems to exhibit responsive movements at the meter scale. To the best of our knowledge, the presented structures constitute the first examples of large-scale self-shaping with differentiated substructures as inspired by biological materials. Through an integrative approach of hybrid additive fabrication, we combine the actuating behavior of wood bilayers with the physical programmability of extrusion-based 3D-printing. To encode the desired material properties and behaviors, we have developed a material programming method for tailoring 3D-printed meta-structures and embedding HWAs using robotic fabrication. We introduce the parameters for tuning mechanical properties (e.g. compliance and elasticity of varying magnitudes and anisotropies) and assess the tectonic interface between the natural and meta-materials. Finally, we detail the sequential process of multi-material and multi-tool hybrid additive fabrication in an industrial setting.

The physical material and fabrication logic, rather than any electronics or digital control, dictate the self-shaping behaviors of the biocomposite material system. These adaptive systems allude to the potential for buildings to become more in tune with the fluctuating environment. Biocomposite elements that self-shade

Table A1. Specifications of the HWA manufacturing as used in this project.

Layer	Wood species	Height h [mm]	Orientation[a]	E modulus [Mpa]	Swelling coefficient α	Starting WMC [%]	Ending WMC [%]	Radius ρ [mm]
Active	Maple	11	90°	1700	0.0016	25	10	420
Passive	Maple	3	0°	14 000	0.0001			

[a]As a result of the orientation, the active layers take into account the radial direction, whereas the passive layers take into account the longitudinal direction.

and self-ventilate without electrical power can serve as a solution to energy-efficient indoor climate control, while autonomously self-forming and self-stiffening biocomposite components present promising applications for the simple and cheap on-site assembly and construction of architectural structures. Through a rearranging of materials across scales, large-scale responsive systems that intelligently interact with their surroundings can be created from natural and sustainable resources.

Acknowledgments

This work was partially supported by the Deutsche Forschungsgemeinschaft (DFG, German Research Foundation) under Germany's Excellence Strategy [EXC 2120/1—390831618] and the Sino-German Center for Research Promotion [GZ 1162]. The authors especially thank Zied Bhiri and BEC GmbH for their extended efforts in robotic extrusion integration.

Data availability statement

The data that support the findings of this study are available upon reasonable request from the authors.

Appendix A. Technical details of the hygroscopic wood actuator design

We designed the HWA's curvature using a model derived from the Timoshenko theory of predicting bending in bimetallic thermostats (Timoshenko 1925) adapted for modeling wood bilayers (Rüggeberg and Burgert 2015) as a function of change in WMC.

Where $c - c_0$ is the WMC change, α is the differential swelling coefficient, H is the total bilayer thickness, and h and E are the height and elastic modulus of each layer according to their respective orientations, the single direction (cylindrical) curvature is calculated as:

$$\frac{1}{\rho} = \frac{6(1+m)^2}{\left(3(1+m)^2 + (1+mn)\left(m^2 + \frac{1}{mn}\right)\right)} \times \frac{(\alpha_2 - \alpha_1)(c - c_0)}{H}$$

$$m = \frac{h_1}{h_2}, \qquad n = \frac{E_1}{E_2}.$$

The flat state of the HWA is programmed through the WMC of the active layer of boards at the time of HWA manufacturing. Therefore, by tuning the WMC of the active layer, HWAs can be calibrated to link a specific curvature to a determined RH level. We designed our HWAs to be flat at equalization to a high RH environment (with a WMC of 25%) and curved at equalization to dry, ambient conditions (with a target WMC of 10%).

Sycamore maple (*Acer pseudoplatanus*) was used for all the presented experiments. We calculated the specifications for each layer of boards according to reference values from literature (Sonderegger *et al* 2013 and Rijsdijk and Laming 2010), for attaining a predicted radius of 420 mm.

Appendix B. Robotic code organization

The code for robotic production was written in the KUKA robot language and organized in a modular structure of `.src` files. A main program file was automatically generated along with the associated subroutine files to be executed in the correct sequence. The following pseudocode outlines the basic program steps that were taken during the hybrid additive fabrication procedure:

```
DEF Main()
    Robot Initialization
    DEF Print()
        PickupExtruder()
        Extruder Initialization
        Purge Material
        Print Base Layers...
        StoreExtruder()
    END
    DEF Place()
        PickupGripper()
        foreach HWA do
            Grip HWA...
            Insert HWA...
        end
        StoreGripper()
    END
    DEF Print()
        PickupExtruder()
        Extruder Initialization
        Purge Material
        Print Top Layers...
        StoreExtruder()
    END
END
```

ORCID iDs

Tiffany Cheng https://orcid.org/0000-0002-0596-5587
Dylan Wood https://orcid.org/0000-0003-0922-5399
Achim Menges https://orcid.org/0000-0001-9055-4039

References

Bergman R D and Bowe S A 2008 Environmental impact of producing hardwood lumber using life-cycle inventory *Wood Fiber Sci.* **40** 448–58

Breiner T A, Quarles S L, Huber D W and Arganbright D G 1987 Steam and electrical consumption in a commercial scale lumber dry kiln (May 20-22 Corvallis, Oregon) *Western Dry Kiln Association* pp 83–94

Cheng T, Tahouni Y, Wood D, Stolz B, Mülhaupt R and Menges A 2020 Multifunctional mesostructures: design and material programming for 4D-printing *SCF '20: Symp. on Computational Fabrication (Virtual Event USA)* ed E Whiting, J Hart, C Sung, N Peek, M Akbarzadeh, D Aukes, A Schulz, H Taylor and J Kim (New York: ACM) pp 1–10

Cheng T, Wood D, Wang X, Yuan P F and Menges A 2020 Programming material intelligence: an additive fabrication strategy for self-shaping biohybrid components *Biomimetic and Biohybrid Systems* (*Lecture Notes in Computer Science*) ed V Vouloutsi, A Mura, F Tauber, T Speck, T J Prescott and P F M J Verschure vol 12413 (Berlin: Springer) pp 36–45

Correa D, Papadopoulou A, Guberan C, Jhaveri N, Reichert S, Menges A and Tibbits S 2015 3D-printed wood: programming hygroscopic material transformations *3D Print. Addit. Manuf.* **2** 106–16

Dawson C, Vincent J F V and Rocca A-M 1997 How pine cones open *Nature* **390** 668

Dow T A and Scattergood R O 2003 Mesoscale and microscale manufacturing processes: challenges for materials, fabrication and metrology *Proc. of the ASPE Winter Topical Meeting* vol 28 (American Society for Precision Engineering) pp 14–9

Eder M, Schäffner W, Burgert I and Fratzl P 2020 Wood and the activity of dead tissue *Adv. Mater.* e2001412

El-Sehily B M 2016 Fracture mechanics in ancient Egypt *Procedia Structural Integrity* **2** 2921–8

Frey M, Widner D, Segmehl J S, Casdorff K, Keplinger T and Burgert I 2018 Delignified and densified cellulose bulk materials with excellent tensile properties for sustainable engineering *ACS Appl. Mater. Interfaces* **10** 5030–7

Grönquist P, Panchadcharam P, Wood D, Menges A, Rüggeberg M and Wittel F K 2020 Computational analysis of hygromorphic self-shaping wood gridshell structures *R. Soc. Open Sci.* **7** 192210

Grönquist P, Schnider T, Thoma A, Gramazio F, Kohler M, Burgert I and Rüggeberg M 2019 Investigations on densified beech wood for application as a swelling dowel in timber joints *Holzforschung* **73** 559–68

Grönquist P, Wood D, Hassani M M, Wittel F K, Menges A and Rüggeberg M 2019 Analysis of hygroscopic self-shaping wood at large scale for curved mass timber structures *Sci. Adv.* **5** eaax1311

Harlow W M, Côté W A and Day A C 1964 The opening mechanism of pine cone scales *J. For.* **62** 538–40

La Magna R and Knippers J 2018 Tailoring the bending behaviour of material patterns for the induction of double curvature *Humanizing Digital Reality* ed K de Rycke, C Gengnagel, O Baverel, J Burry, C Mueller, M M Nguyen, P Rahm and M R Thomsen vol 31 (Berlin: Springer) pp 441–52

Langhansl M, Dörrstein J, Hornberger P and Zollfrank C 2021 Fabrication of 3D-printed hygromorphs based on different cellulosic fillers *Functional Composite Materials* **2** 1

Lewis J A, Bell M A, Busbee T A and Minardi J E 2016 Printed three-dimensional (3D) functional part and method of making *US Patent Specification* 2016/0198576A1

Megaro V, Zehnder J, Bächer M, Coros S, Gross M and Thomaszewski B 2017 A computational design tool for compliant mechanisms *ACM Trans. Graph.* **36** 1–12

Menges A and Reichert S 2015 Performative wood: physically programming the responsive architecture of the hygroscope and hygroskin projects *Archit. Des.* **85** 66–73

Panetta J, Zhou Q, Malomo L, Pietroni N, Cignoni P and Zorin D 2015 Elastic textures for additive fabrication *ACM Trans. Graph.* **34** 1–12

Poppinga S, Nestle N, Šandor A, Reible B, Masselter T, Bruchmann B and Speck T 2017 Hygroscopic motions of fossil conifer cones *Sci. Rep.* **7** 40302

Poppinga S, Zollfrank C, Prucker O, Rühe J, Menges A, Cheng T and Speck T 2018 Toward a new generation of smart biomimetic actuators for architecture *Adv. Mater.* **30** e1703653

Raney J R and Lewis J A 2015 Printing mesoscale architectures *MRS Bull.* **40** 943–50

Redlich O 1970 Intensive and extensive properties *J. Chem. Educ.* **47** 154

Reichert S, Menges A and Correa D 2015 Meteorosensitive architecture: biomimetic building skins based on materially embedded and hygroscopically enabled responsiveness *Comput. Aided Des.* **60** 50–69

Rijsdijk J F and Laming P B 2010 *Physical and Related Properties of 145 Timbers. Information for Practice* (Berlin: Springer) p 385

Rowell R M 2012 Moisture properties *Handbook of Wood Chemistry and Wood Composites* ed R M Rowell (Boca Raton, FL: CRC Press) pp 77–97

Rüggeberg M and Burgert I 2015 Bio-inspired wooden actuators for large scale applications *PloS One* **10** e0120718

Sonderegger W, Martienssen A, Nitsche C, Ozyhar T, Kaliske M and Niemz P 2013 Investigations on the physical and mechanical behaviour of sycamore maple (*Acer pseudoplatanus L.*) *Eur. J. Wood Wood Prod.* **71** 91–9

Tahouni Y, Cheng T, Wood D, Sachse R, Thierer R, Bischoff M and Menges A 2020 Self-shaping curved folding *SCF'20: Symp. on Computational Fabrication (Virtual Event USA)* ed E Whiting, J Hart, C Sung, N Peek, M Akbarzadeh, D Aukes, A Schulz, H Taylor and J Kim (New York: ACM) pp 1–11

Thoma A, Adel A, Helmreich M, Wehrle T, Gramazio F and Kohler M 2019 Robotic fabrication of bespoke timber frame modules *Robotic Fabrication in Architecture, Art and Design 2018* ed J Willmann, P Block, M Hutter, K Byrne and T Schork vol 61 (Berlin: Springer) pp 447–58

Tibbits S 2014 4D printing: multi-material shape change *Archit. Des.* **84** 116–21

Timoshenko S 1925 Analysis of bi-metal thermostats *J. Opt. Soc. Am.* **11** 233

Vailati C, Bachtiar E, Hass P, Burgert I and Rüggeberg M 2018 An autonomous shading system based on coupled wood bilayer elements *Energy Build.* **158** 1013–22

Valentine A D *et al* 2017 Hybrid 3D printing of soft electronics *Adv. Mater.* **29** 40

Willmann J, Knauss M, Bonwetsch T, Apolinarska A A, Gramazio F and Kohler M 2016 Robotic timber construction—expanding additive fabrication to new dimensions *Autom. Constr.* **61** 16–23

Wood D M, Correa D, Krieg O D and Menges A 2016 Material computation-4D timber construction: towards building-scale hygroscopic actuated, self-constructing timber surfaces *Int. J. Architect. Comput.* **14** 49–62

Wood D, Vailati C, Menges A and Rüggeberg M 2018 Hygroscopically actuated wood elements for weather responsive and self-forming building parts—facilitating upscaling and complex shape changes *Constr. Build. Mater.* **165** 782–91